

CHAPTER 22

ORIGIN, EFFECT AND SUPPRESSION OF SECONDARY WAVES

by C.H. Hulsbergen *

1 Abstract

Beach profile formation may be severely affected by secondary waves which, together with the basic wave, always originate from a sinusoidally-moving wave board. The ascertainment of this experimental fact is followed by an investigation of the behaviour of the generated waves and their interactions. It appears that the many characteristic features, among which the spatial beat phenomenon and the secondary crest formation, are generally in good accordance with the theories of Fontanet [14], and Kravtchenko and Santon [20]. It is concluded that an "outer" analysis, e.g. by plotting the $x-t$ lines of visible peaks, is only of limited use to describe the "inner" character of the complex phenomenon. The subsequent study of the effect of secondary waves on a horizontal sand bed reveals that not only the wave form, but also the sand transport varies spatially, resulting in the formation of bars and troughs. This typical behaviour of the onshore-offshore transport is provisionally investigated in a small pulsating water block. Finally, a method is described which suppresses the secondary waves, by using a low rectangular sill on the otherwise horizontal bottom.

2 Introduction

Secondary waves, solitons, or disturbing waves are three different names for a peculiar kind of wave phenomenon which has been reported under various conditions. All descriptions mention that a regular progressive wave or swell is accompanied by one or more extra wave crests of a smaller height and with a lower propagation speed. Secondary waves have been reported in laboratory experiments with non-breaking waves over a horizontal bed [4,5,11,15,16,18,24,25,31], on a slope or near an abrupt variation in depth, with or without breaking [13,16,19,24,26,27,30], under natural conditions [6,10], [21], and in analytical or numerical computations [7,8,12,14,20,23,24,32,35]. The existence of the phenomenon is no longer a matter of dispute, although in its outer appearance it has sometimes been confused with the - real - wave reflection or with the - non real - "crête secondaire" of Miche [18]. With respect to the origin and the nature of secondary waves, however, no common opinion or complete theory exists as yet, in which situation various deviating interpretations have been put forward. This paper is mainly confined to the case of progressive waves over a horizontal bottom, generated by a sinusoidally-moving piston-type wave board. It combines some experimental results with existing - but partly

* Project engineer, Delft Hydraulics Laboratory, The Netherlands

forgotten - theories, trying to describe and understand the observed phenomena.

In 1969 the starting point for this study was the experimentally-observed fact that beach profile formation may severely be affected by secondary waves. Fig. 1 shows three beach profiles which all had developed to entirely different equilibrium positions in identical wave channels under the same wave conditions. The profiles appeared to be strongly influenced by the sand bars and troughs, which had developed from the originally horizontal section of the bed. This bar system, although being outside the breaker zone, controlled to a great extent the position and the type of breaking, and thus the water movement and sand transport in the surf zone. The formation and the geometry of the bar system, which was not caused by wave reflection, seemed to correspond with and to intensify the secondary surface waves which had been present from the beginning, although they were hardly visible then. Apparently, these small secondary waves originated at the wave board, and a set of experiments were conducted in order to establish the exact nature of the produced waves.

3 Origin and behaviour of secondary waves

3.1 Experimental conditions and measuring procedure

The tests were conducted in two different wave channels, 1.24 m and 0.91 m wide, with smoothly finished sides and bottoms. The lengths of the horizontal sections were 9 m and 13 m respectively, and both channels ended with a 1 in 20 sloping beach as a wave absorber. No other wave absorbers or filters were used. A vertical board, sinusoidally oscillating in a horizontal plane, was used as a wave generator. Wave periods T varied from 1.15 s to 1.92 s, the water depth h varied from 0.10 m to 0.55 m, and the wave height H varied between 0.02 m and 0.15 m. The water depth to wave length ratio h/L thus varied from 0.05 to 0.20, and the Ursell parameter $Ur = HL^2/h^3$ varied between 2 and 104. In general four different wave board strokes were chosen for each h/L -value. The wave form was measured in the centre line of the channel in points 0.2 m apart over a distance of at least 6 m, starting near the wave board. A harmonic analysis yielded the local amplitudes of the first, second, third and fourth harmonic components a_1, a_2, a_3 and a_4 , averaged over three wave periods. The resulting regular spatial variation of a_n , an example of which is presented in fig. 2, forms the essential basis for a further analysis.

3.2 Two different interpretations

The typical wave farms did not differ from those reported earlier, e.g. [5,15,16]. An almost sinusoidal wave farm near the wave generator deforms, while propagating, gradually into a non-symmetric one, with a small hump behind the main crest. This hump may develop, depending on the value of U_r , into a definite secondary crest, located in the trough of the main wave. On that location, the wave farm is symmetric again with respect to the crests. Further downwave this process is repeated in reverse, until the appropriate sine farm is reached again, etc. (see fig. 3). At any fixed place the wave farm is constant in time. At a first glance, one could take the hump or secondary crest as an extra wave, having the same period as the main wave, and propagating with a lower speed because of the difference in wave heights. According to this viewpoint, e.g. [15,16,24], both waves should be just in phase at the locations where a sine wave results, which has a smaller height than at all other locations. The incorrectness of this viewpoint may be demonstrated by the following argument: if the difference in height would be the only reason for the difference in celerity, there would be no reason at all for the sine wave to change its form, because at that location both waves would have the same height, period, and water depth, and thus the same celerity. According to a different point of view [18,23], the symmetrical wave farm with the secondary crest should be regarded as a superposition of the main wave with period T and a smaller wave with period $T/2$, the so-called second harmonic free wave. One crest of this smaller wave contributes to the visible secondary crest, while its other crest coincides with the main wave crest and makes it higher than normal. Thus, the second harmonic free wave is here exactly in phase with the second harmonic component of the basic wave. The resulting sine wave, on the other hand, is caused by the fact that the free and the coupled second harmonic waves are exactly out of phase and are almost cancelled out. Care must be taken, however, not to be misled by the outer appearance of the waves. In general, the visible peaks do not correspond to the crests of real waves, simply because a recorded wave farm has no own identity as soon as it must be regarded as the summation of more than one participating wave. This second point of view agrees well with what may be expected on the basis of literature.

3.3 Theoretical considerations

Fantnet [14] predicts the amplitude and the phase of the second harmonic free wave, which is always the by-product of a sinusoidally-moving piston-type wave board (fig 4). For low h/L -values the free and the coupled second harmonic waves are virtually 180° out of phase. Kravtchenko and Santon [20] predict the generation and the interesting behaviour of a set of two waves, generated by two interacting free waves, with T_1, C_1, L_1, A_1 and T_2, C_2, L_2 and A_2 as period, celerity, length and amplitude, respectively. The new interaction waves have periods defined by the sum and difference frequencies of the interacting waves:

$$1/T_{\star} = |1/T_1 - 1/T_2| \text{ and } 1/T_{\star}' = 1/T_1 + 1/T_2 \tag{3-1}$$

The corresponding celerities are

$$C_{\star} = L_1 L_2 (T_1 - T_2) / T_1 T_2 (L_1 - L_2) \text{ and } C_{\star}' = L_1 L_2 (T_1 + T_2) / T_1 T_2 (L_1 + L_2) \tag{3-2}$$

The corresponding amplitudes are given by

$$A_{\star} = A_1 A_2 \gamma_{1,2} \text{ and } A_{\star}' = A_1 A_2 \eta_{1,2} \tag{3-3}$$

where $\gamma_{1,2}$ and $\eta_{1,2}$, non-dimensionless coefficients of interaction, are very lengthy functions of L_1, L_2 and h [20].

So the interacting basic wave (period T) and Fantnet wave (period $T/2$) produce two extra waves with periods $T_{\star} = T$ and $T_{\star}' = T/3$ according to (3-1), whereas their celerities C_{\star}, C_{\star}' and amplitudes A_{\star}, A_{\star}' are given by (3-2) and (3-3). As an example, fig 5 presents the values of $\gamma_{1,2}, \eta_{1,2}$ and $\eta_{1,2}'/\gamma_{1,2}$ as a function of h/L_1 for $T_1 = 1.56s$ and $T_2 = 0.78s$. The basic wave is regarded as a third-order Stokes wave, i.e. composed of three harmonic components, with amplitudes A_1, A_2' and A_3' , all propagating with the same celerity C_1 of the basic wave.

We have, then, six different "waves", viz. three pairs of waves with periods $T, T/2$ and $T/3$ respectively. In each pair both waves thus have equal periods T/n ($n = 1, 2, 3$), but different celerities (fig 6). Each pair can of course give only a single value of a_n in the harmonic analysis at a specific location, obtained by adding the constituent amplitudes as vectors. Each resulting amplitude a_n must then theoretically display a rhythmic spatial behaviour. Its maximum and minimum values are the sum and the difference, respectively, of the amplitudes of the participating "waves". Because of the difference in celerities, the faster wave of the pair will overtake the slower one within a certain distance, the overtake length L_{ov} . It follows immediately that

$$L_{av} = L_{slow} C_{fast} / (C_{fast} - C_{slow}) \tag{3-4}$$

where the subscripts fast and slow refer to the faster and slower wave, respectively.

As an example, fig 7 shows the expected behaviour of a_1 as a function of the phase angle $\varphi(x)$ between the constituent amplitudes A_1 and A_{\star} . It should be noticed that the celerities of a_1 and A_1 are in general not equal.

3.4 Comparison of theory with experiments

The second harmonic amplitude a_2

Supposing that a_2 is the vector summation of the second harmonic Stokes amplitude A_2' and the Fontanet amplitude A_2 , both amplitudes follow from the maximum and minimum a_2 values (see figs 2,7):

$$\text{Stokes 2nd order: } A_2' = (a_{2\max} + a_{2\min})/2 \quad . \quad .(3-5)$$

$$\text{Fontanet} \quad : A_2 = (a_{2\max} - a_{2\min})/2 \quad . \quad .(3-6)$$

provided that $A_2' \geq A_2$, which is true according to Fontanet [14]. In fig. 8 the experimentally determined value of A_2' , A_2 and A_2/A_2' have been plotted, together with the respective theoretical curves of Miche [28] and Fontanet [14]. The fact that $a_{2\min}$ is always found near the wave board (fig 2) is in support of Fontanet's phase relationship (fig 4). From (3-4) it follows for the overtake length of a_2 :

$$L_{ov2} = L_2 C_1 / (C_1 - C_2) \quad . \quad .(3-7)$$

or in dimensionless form:

$$L_{ov2}/L_1 = C_2/2(C_1 - C_2) \text{ or } L_{ov2}/L_1 = L_2/(L_1 - 2L_2) \quad . \quad .(3-8)$$

The measured and theoretical values of L_{ov2}/L_1 have been plotted in fig 9, which show a reasonable agreement. For relatively deep water, $L_1 = 4L_2$ and $C_1 = 2C_2$, so that from (3-8):

$$L_{ov2} = L_1/2 \quad . \quad .(3-9)$$

In this case, the overtake length is apt to be mixed up with the reflection phenomenon. For shallow water conditions, $(C_1 - C_2)$ diminishes to very small values (see fig 6) which would give very long overtake lengths according to (3-8). However, in shallow water the celerity increases with the wave height, which affects C_1 more than C_2 . Therefore, the denominator in (3-8) is increased remarkably, causing the overtake length to decrease, if C_1 increases only slightly. So in order to find the correct value of L_{ov} , one must insert the correct (wave height adapted) values of C and L in (3-8). In fig. 9 the 3rd order Stokes theory [34] was used to find L_{ov2}/L_1 for $H/h = 0.4$, but a cnoidal theory may perhaps work out better. In view of the difficulty to measure the exact celerity of a wave, especially when secondary waves are present, the argument may be reversed in that from (3-7) and from the exactly-measurable overtake length the proper wave celerity can be determined:

$$C_1 = L_{ov2} C_2 / (L_{ov2} - L_2) \quad . \quad .(3-10)$$

The first harmonic amplitude a_1

From fig 2 it appears that L_{ov1} is equal to L_{ov2} . When the theoretical expressions for C_1 , C_x , L_1 and L_x are substituted in (3-4), it follows that $L_{ov1}/L_1 = L_2/(L_1 - 2L_2)$, so that indeed $L_{ov1} = L_{ov2}$. The experiments (fig 2) show that a_{1max} is always found near the wave board; the theory [20] is not clear on this point. In order to determine A_1 and A_x from the experimental values of a_{1max} and a_{1min} , the wave reflection must be taken into account, because reflection alone also causes a certain variation in a_1 . With respect to A_1 , reflection does not interfere and the normal formula holds:

$$A_1 = (a_{1max} + a_{1min})/2 \quad . \quad (3-11)$$

According to [17] the reflection coefficient is about 5 %, and especially for $Ur < 28$ the reflection appeared to be the dominating feature, causing much scatter. So only for $Ur > 28$ the values of A_x have been determined as

$$A_x = (a_{1max} - a_{1min})/2 - 0.05 A_1 \quad .. \quad (3-12)$$

Fig 10 shows for the larger values of h/L_1 a remarkable discrepancy between $A_{x,experim.}$ according to (3-12) and $A_{x,theor}$ according to (3-3). The reason may be that the magnitude of A_x , which is only a few mm, is small compared to the disturbing influence of reflection.

The third harmonic amplitude a_3

From the experimental results (fig 2) it appears that a_3 has a similar spatial behaviour as a_2 . Indeed, when the theoretical values for C_1 , C_x' , L_1 and L_x' are substituted in (3-4), the result is again that $L_{ov3} = L_{ov2}$, so

$$L_{ov1} = L_{ov2} = L_{ov3} \quad . \quad (3-13)$$

One complication appears in the behaviour of a_3 . For the higher Ur -values (fig 2, run 30), there seems to be an extra, smaller overtake length, apparently caused by yet another wave with period $T/3$. This might be a third order free wave, generated by the wave board in analogy with Fontanet's wave, but no information exists with respect to such a wave. So a certain error must be accepted in determining the amplitudes A_3' and A_x' according to

$$A_3' = (a_{3max} + a_{3min})/2 \quad . \quad (3-14)$$

and $A_x' = (a_{3max} - a_{3min})/2 \quad . \quad (3-15)$

For the lower Ur -values, a_3 is so small (order 1 mm) that a further analysis is useless in view of the scatter. Therefore, only those results were used in (3-15) for which $A_3' \geq 2$ mm. A reasonable agreement is shown to be present in fig. 11 between A_{\star}' experim. and A_{\star}' theor., although there is considerable scatter. The ratio A_{\star}'/A_3' has been plotted in fig. 12; it displays a similar trend as A_2/A_2' in fig. 8.

The fourth harmonic amplitude a_4

The harmonic analysis was done for four harmonics, but a_4 was so small that it has not been plotted. As an average value, it may be stated that the magnitude of a_4 was about 50% of a_3 .

3.5 The wave form

The presence of a number of waves with different celerities, predicted by the combined theories and confirmed by the experiments, has as a consequence that the wave form varies from place to place. The wave form at any place is predictable if the amplitudes, the celerities and the initial phase-angles of all participating waves are known. From section 3.4 it follows that this is indeed the case to a certain degree of accuracy, especially for the celerity and the initial phase angles. An example of a resulting $x-t$ diagram for the participating wave crests is given in fig. 13 for $h/L_1 = 0.10$, with the following relative celerities (compare fig. 6):

$$C_2/C_1 = 0.821, \quad C_{\star}/C_1 = 0.695 \quad \text{and} \quad C_{\star}'/C_1 = 0.868$$

Near the wave board, indicated as place no. 1, the six waves are phased as follows:

$$\left. \begin{array}{l} A_1 \text{ and } A_{\star} \text{ are in phase} \\ A_2' \text{ and } A_2 \text{ are } 180^\circ \text{ out of phase} \\ A_3' \text{ and } A_{\star}' \text{ are } 180^\circ \text{ out of phase} \end{array} \right\} \text{ place no. 1, } x = 0 \quad \dots (3-16)$$

With increasing x the initially symmetric wave form loses its symmetry, because the phase-relation (3-16) changes. But as soon as the crest of A_2 and A_{\star}' has just been overtaken by the corresponding harmonic components of the basic wave, another symmetric wave results, quite different from (3-16).

$$\left. \begin{array}{l} A_1 \text{ and } A_{\star} \text{ are } 180^\circ \text{ out of phase} \\ A_2' \text{ and } A_2 \text{ are in phase} \\ A_3' \text{ and } A_{\star}' \text{ are in phase} \end{array} \right\} \text{ place no. 2, } x = L_0\sqrt{2} \quad \dots (3-17)$$

Because the basic wave is faster than any other wave, firstly same undisturbed basic waves will pass along a certain point far enough from the wave board. Then, as the slower waves reach this point one by one, the wave farm will be unstationary for some time. Only after the arrival of the slowest wave, a new stationary wave develops, now containing all disturbing waves together with the basic wave [3]. So the basic wave of permanent farm is always present, but generally not in an explicitly visible form. Starting for example from the conditions $h/L_1 = 0.10$, $H/h = 0.36$ and $T_1 = 1.56s$, the following amplitudes result from section 3.4:

$$\begin{array}{l}
 A_1 = 3.82 \text{ cm} \\
 A_{2'} = 1.72 \text{ cm} \\
 A_{3'} = 0.79 \text{ cm} \\
 A_2 = 1.24 \text{ cm} \\
 A_{*} = 1.44 \text{ cm} \\
 A_{*' } = 0.73 \text{ cm}
 \end{array}
 \left. \begin{array}{l}
 \\
 \\
 \\
 - \\
 \\
 \end{array} \right\}
 \begin{array}{l}
 \text{3rd order Stokes wave, basic wave} \\
 \\
 \text{2nd harmonic free wave (Fantenet)} \\
 \text{interaction waves (Krivtchenka and Santan)}
 \end{array}$$

Based on the experimental results in figs 10 and 11, A_{*} and $A_{*'}$ have been reduced to 0,965 cm and 0,635 cm, respectively. With these amplitudes, and their phase relationships from fig 13, various wave farms were reconstructed in fig. 14 for place no. 1, place no. 2 and 9 intermediate locations; for comparison also the undisturbed basic wave has been plotted. Obviously, the crest of the composed wave farm does in general not coincide with the crest of the basic wave, nor is a secondary crest identical with the crest of one of the participating smaller waves. Two more comments may be made on figs. 13 and 14. Firstly, the total wave height varies and has a minimum at place no. 1 and a maximum near place no. 2. Secondly, a horizontal section through the x-t diagram results in an instantaneous wave surface which shows in general no regular spatial recurrence system, because the overtake length is in general not a multiple of the various wave lengths involved.

Of all locations, places no. 1 and 2 display the most characteristic wave farms, which will be analyzed in some detail.

At place no. 1, $x = k L_{av}$, where $k = 0, 1, 2, 3, \dots$. Here practically a sine wave results, consisting mainly of A_1 and A_{*} , a_1 being maximum; a_2 and a_3 reach their minimum values. Of all measured values, the following averages result:

$$a_{2min}/a_{1max} = 0.10 \text{ and } a_{3min}/a_{1max} = 0.027.$$

At place no. 2, $x = (k + 1/2) \cdot L_{ov}$ where $k = 0, 1, 2, 3, \dots$. Here the resulting wave is far from sinusoidal, a_1 being minimum and both a_2 and a_3 being maximum. Of all measured values in this place, the ratios a_{2max}/a_{1min} and a_{3max}/a_{1min} have been plotted in fig. 15 as a function of Ur . Two lines have been drawn to represent these points and an additional line in agreement with section 3.4 represents the fourth harmonic. On the basis of these lines, and taking into account the relevant phase relationship (3-17), wave forms were constructed for various values of Ur (fig. 16). For $Ur \geq 13$ a secondary crest exists in the trough centre, which is in accordance with Madsen's value of $4\pi^2/3$ [23]. These "reconstructed" wave forms may be compared with experimental wave forms recorded in place no. 2, presented in fig. 17. For both figures 16 and 17 the relative height of the secondary crest increases with Ur as shown in fig. 18, where also some of Golvin's results [15] have been plotted. The discrepancy between the reconstructed and the direct experimental values of H'/H_{tot} may partly be due to the fact that, especially for higher Ur -values, 5th and higher harmonic components do participate in fig. 17, but not in fig. 16.

4 Influence of secondary waves on a horizontal sand bed

Considering sand transport, the behaviour of the orbital motion near the bed is of more direct relevance than the fluid surface [1]. Simultaneous measurements of the wave profile and the orbital velocity near the bed carried out in a long wave channel with a fixed horizontal bottom, revealed that their behaviour is virtually the same (fig. 19). This is substantiated by a harmonic analysis of the orbital velocity, plotted as a function of the distance from the wave board (fig. 20). The regular spatial behaviour of the orbital velocity field must have as a consequence that the onshore-offshore sand transport varies spatially, too. In order to check this, tests were run in a 1.20 m wide wave channel, with a smooth horizontal concrete bottom over the first section of 2 m from the wave board. A horizontal flat sand bed extended over the next 9 m, terminating in a 1 on 20 sloping spending beach. Fig. 21 shows the experimental conditions and the resulting bed forms. Ur varied from 40 to 57. The wave lengths produced in the sand bed are very clearly equal to the respective overtake lengths. In test T73-1, a bar-trough system with a smaller reference length, caused by wave reflection, is superimposed on the large scale bar system. Looking back from these results to fig. 1, the cause of the undulating bed profile is clear now, realising that L_{ov} is approx. 3.20 m for the given conditions. These bars, once formed from an initially flat bed, may on their turn provoke new secondary

waves, which all interfere with the breaker type and breaker location, the water circulation, and the morphological development in the surf zone and on the beach. On certain occasions, the undulations have even been seen to develop into large breaker bars. Although the drastic influence of the disturbing waves, via the formation of bars and troughs, on the beach profile development was quite clear in the case under consideration, it is also clear that such an influence may be present without recognizing it as such, so that a general warning seems useful here. For instance, from Bognold's clear description [2, p461 etc] it can safely be concluded that he was confronted with similar phenomena in his tests. On the other hand, the interrelation between secondary waves, bar systems and beach behaviour seems not to be restricted to model experiments [22], so that the present study may be of a more general application. Therefore, the bed profiles in fig. 21 have been converted into a rate of transverse sand transport by using the sand balance. Fig. 22 shows the result for T73-2, where also the wave form is presented for various locations. For $x = 5$ m, one overtaken length from the wave board, the sinusoidal motion has no preference for a certain direction, and consequently the sand transport rate is zero. In general, the magnitude and the direction of the sand transport appears to be remarkably dependent on slight differences in the wave form.

5 Experiments in a pulsating water block

5.1 Apparatus and procedure

In order to study the effect of higher harmonic components in the orbital motion on the transverse sand transport, some preliminary tests were run in a very simple and small pulsating water block. This apparatus, originally on idea of Silvester [29, 33] consists of a bottomless perspex box, forced by a programmable wave generator to oscillate over a bed (fig. 23). In this bed, a sand bed and two sand traps are installed. The block moves under water in a perspex tank. Before each test, the sandbed is smoothed and made flush with the fixed bed. The tests are divided into periods of 5 minutes, after which the trapped sand is collected in order to define the net sediment transport rate and direction. Ripples are formed in the first 1 or 2 minutes, sometimes staying in fixed positions, sometimes moving, but not necessarily in the same direction as the net sediment transport.

5.2 Test results

Throughout the tests, a basic period of 1.40 s was used, with an amplitude $A_1 = 0.05$ m. In the first series of tests, of 15 min. each, the influence of the 2nd harmonic component A_2 was investigated. With a sinusoidal movement, an almost zero net transport is found, as expected (fig. 24). By adding the second harmonic component with $A_2/A_1 = 5\%$ and 10% , respectively, and with the same phase relationship ($\varphi_2 = 0$) as occurs in a 2nd order Stokes wave, a marked influence appears on the transport pattern. By visual observation, this was caused by the circumstance that vortex formation and behaviour is very sensitive to the form of the orbital velocity. The corresponding velocity is also shown in fig. 24.

In a second series of tests of 25 min. each, a second harmonic component with $A_2/A_1 = 20\%$ was added, but now with a phase relation varying from $\varphi_2 = 0^\circ$ (like in a 2nd order Stokes wave) to $\varphi_2 = 90^\circ$ (fig. 25). The resulting sand transports for two sand diameters are presented in fig. 26. Clearly, these are all only quite preliminary results, both qualitatively and quantitatively speaking, and further tests with better equipment are planned. Nevertheless, it seems that this very close dependence of the direction and the rate of transverse sand transport on slight variations in the wave form and the orbital velocity field, is important for any basic study of beach profile development.

6 Suppression of secondary waves

In order to suppress the parasitic waves, Biésel and Suquet [4] suggested already in 1951 to use a more realistic motion of the wave board than a simple harmonic oscillation. Work along this line has recently led to encouraging results [9,23]. Also a different method may be thought of, which has provisionally been tested. In this method, the experimental fact is used that a bar or sill, placed on the horizontal bottom of a wave channel, generates free higher harmonic waves when regular waves proceed over it. [16,19,27]. No theory being available on this subject, a trial and error method was used in order to find a sill of such dimensions and on such a location, that it would produce a second harmonic free wave of the same height and exactly 180° out of phase with respect to the Fontanet wave. One of the results is presented in figs. 27 and 28, giving the characteristics of the sill, the wave forms and the harmonic analysis for two runs with the same rectangular sill on two different locations. Without a sill, a secondary

wave was clearly visible. In both cases the influence of the sill - with a thickness of only 0.1 h - was surprisingly great. In run D, a virtually permanent wave farm resulted dawnward from the sill, while a distinct secondary wave was still visible between the wave flap and the sill. This optimum result was obtained with the far end of the sill at a distance of 3 m from the wave flap, corresponding to L_{av} . When the sill was moved to different locations, the resulting wave farm immediately deteriorated. The worst result was obtained for run B, where the sill was shifted over a distance of $L_{av}/2$. This suggests that the overtaking length is an important parameter in determining the optimum sill location, although the physical process is not well understood. By looking at it, a certain analogy seems to exist with the effect of a bulb on the waves generated near a ship's bow.

7 Conclusions

- a. Secondary waves may be generated by the wave board, or may be provoked by a sill, bar, slope, or by breaking waves.
- b. Secondary waves, generated by the wave board, may adequately be described by combining the theories of Fantanet [14], and Kravtchenka and Santan [20].
- c. Secondary waves may have a very pronounced influence on beach profile formation, although this influence may be quite difficult to recognize as such.
- d. The rate and the direction of the transverse sand transport under waves is very delicately dependent of the wave farm, i.e. the form of the orbital velocity field.
- e. An adequately designed sill of rectangular cross-section may be used to suppress the Fantanet wave.

References

1. Adeyema, M. D., 12th C. E. C., chapter 27, 1970.
2. Bagnald, R. A., J. Inst. Engrs., 27, 1947, pp. 447 - 469.
3. Bendykawska, G., Rozprawy Hydratechniczne, 1971, no. 28, pp. 27 - 39.
4. Biésel, F. and Suquet, F., La Haulle Blanche, 1951, no. 2,4,5 and 1952 no. 6.
5. Baczar-Karakiewicz, B., Archiwum Hydratechniki, 19, 1972, no. 2, pp. 197 - 210.
6. Baczar-Karakiewicz, B., Archiwum Hydratechniki, 20, 1973, no. 1, pp. 47 - 58.
7. Baczar-Karakiewicz, B., Rozprawy Hydratechniczne, 1973, no. 32, pp. 51 - 67.

8. Bryant, P. J , J Fl. Mech., 59, 1970, part 4, pp 625 - 644
9. Buhr Hansen, J., and Svendsen, I.A , T.U. Denmark, Inst of Hydr. Eng. progr. rep. 32, 1974, pp 3 - 8
10. Byrne, R. J., J of Geaph. Res , 74, 1969, na. 10, pp 2590 - 2596
11. Caldwell, J M , Pracs 1st Conf an Ships and Waves, 1954
12. Dingemans, M.W., Delft Hydr Lab Repart no. R 729 - II, 1973
13. Flinterman, J , and Stein, T., Delft Hydr Lab , Repart na 08114, 1953
14. Fantanet, P., La Hauille Blanche, 1961, no. 1,2
15. Galvin, C J , CERC-nate an secondary waves, Sept. 1970
16. Gada, Y., et al Part and Harbaur Res Inst Rept na.13, with appendix, 1967
17. Greslou, L , and Mahé, Y , 5th C E C. chapter 7, 1954
18. Hulsbergen, C.H., Delft Hydr. Lab , Res rep. na. S 55 - III, 1972
19. Jalas, P., La Hauille Blanche 1962 na. 6, pp 758 - 769
20. Kravtchenka, J , et Santan, L , 7th Gen. Meeting I.A.H.R. 2, 1957, chapter D2
21. Larras, J , I A H.R , 1963, pp 351 - 352
22. Lau, J., and Barcilan, A , J af Phys Oceanography, 2, 1972, na 4, pp 405 - 410
23. Madsen, O S , J af Geaph. Res 76, 1971, na. 36, pp 8672 - 8683
24. Madsen, O.S , Mei, C.C , and Savage, R P , J Fl.M 44, 1970, part I, pp 195 - 208
25. Marcau, C , Thesis, Univ. af Grenoble 1969
26. Masan, M.A., and Keulegan, C.H , B E.B. Eng. notes, na. 19, Tech. Mem. 5, 1944
27. McNair, E C., and Sarensen, R M , 12th C.E C. chapter 26, 1970
28. Miche, M , Annales des Pans et Chaussées 1944
29. Magridge, G R., ASCE, J. Hydr Div., HY7, 1970, pp 1587 - 1604
30. Onaszka, J , Razprawy Hydratechniczne, 1973, na. 32, pp 69 - 84
31. Santan, L., IVes Jaurnées de l'Hydr , Question III, Rappart 6, 1956
32. Schweigman, C , Delft Hydr. Lab , Res. rep. na S 13, 1965
33. Silvester, R., J af the Inst af Engrs., Austr 37, Oct-Nav 1965, pp 311 - 321
34. Skjelbreia, L., 3rd order Stakes wave tables, Council an wave res 1958
35. Takana, K , La Hauille Blanche, 1960, na. 3, pp 247 - 259

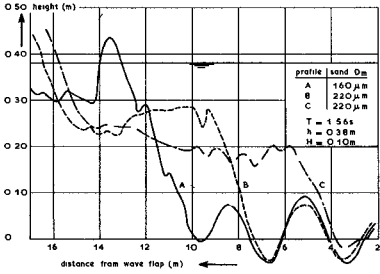


Figure 1: Beach profiles affected by secondary waves

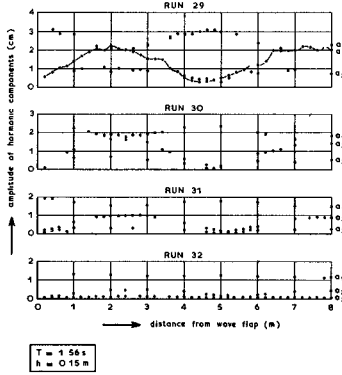


Figure 2: Typical variation of harmonic amplitudes

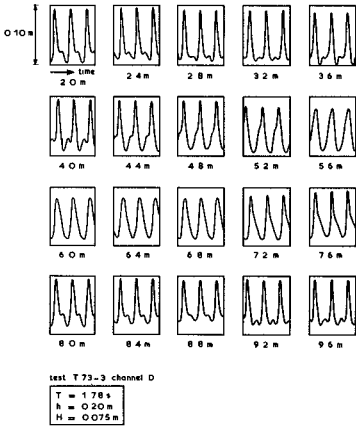
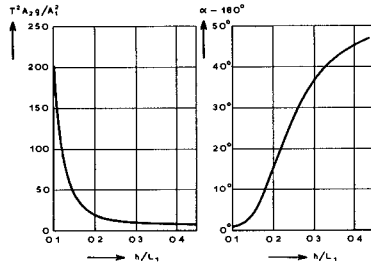


Figure 3: Typical variation of wave farms



T = period of wave board
 A_2 = amplitude of Fantanet wave with period $T/2$
 g = acceleration due to gravity
 A_1 = amplitude of 1st harm component in basic wave with period T
 α = phase lag near wave board between free and coupled 2nd harm components

Figure 4. Characteristics of Fantanet wave

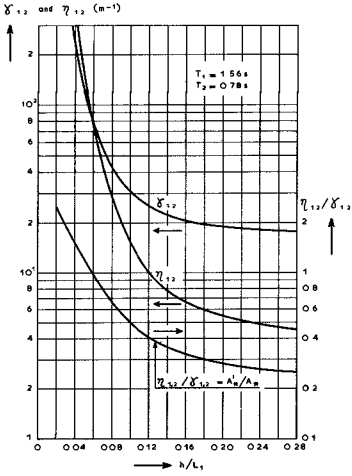


Figure 5: Coefficients of interaction according to Kravtchenko and Sonton

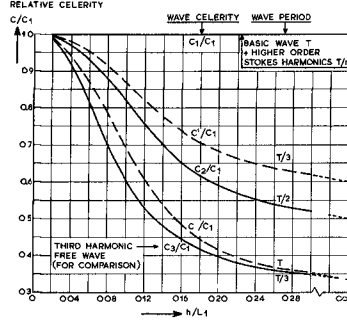


Figure 6: Relative wave celerities; influence of wave height neglected

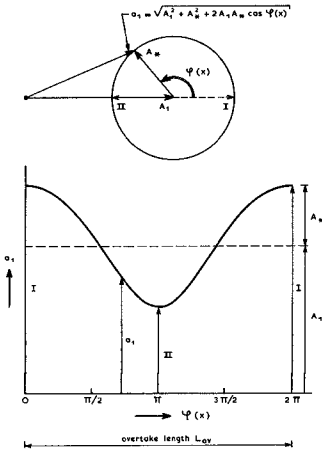


Figure 7: Vector summation of \$A_1\$ and \$A_2\$ and resulting spottial behaviour of \$\sigma_1\$

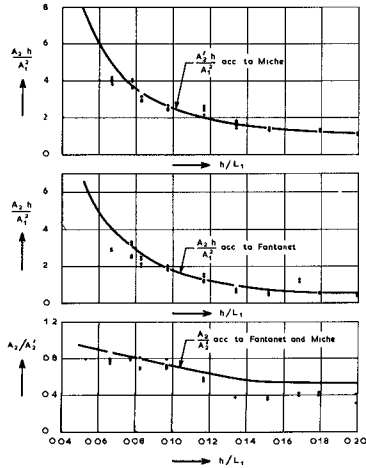


Figure 8: Comparision of theory and experiments for 2nd harmonic components \$A_2\$ and \$A_2'\$

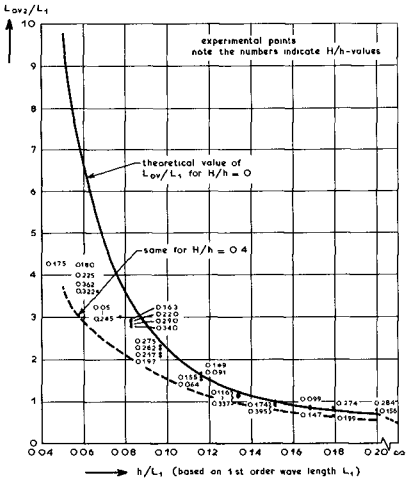


Figure 9: Dimensionless overtake length L_{ov2}/L_1

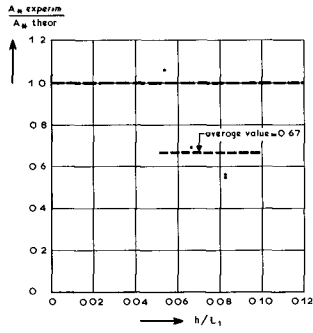


Figure 10: Comparison of theory and experiments for 1st harmonic component A_x

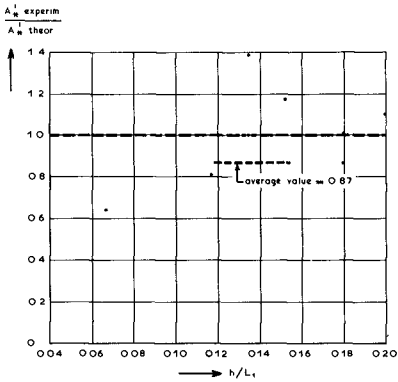


Figure 11: Comparison of theory and experiments for 3rd harmonic component A_x'

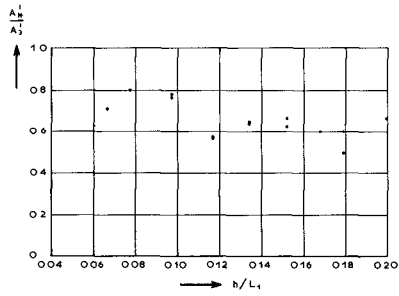


Figure 12: Experimental ratio A_x'/A_3'

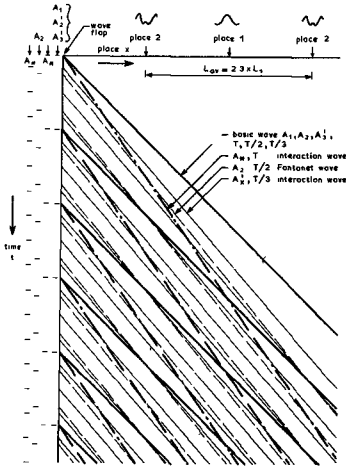


Figure 13: $x-t$ diagram of participating wave crests for $h/L_1 = 0.10$

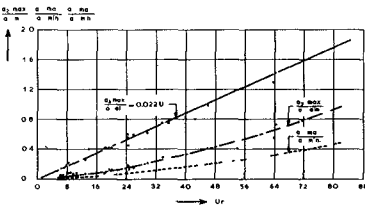


Figure 15: Relative amplitudes at $x = (1/2 + k) L_{av}$

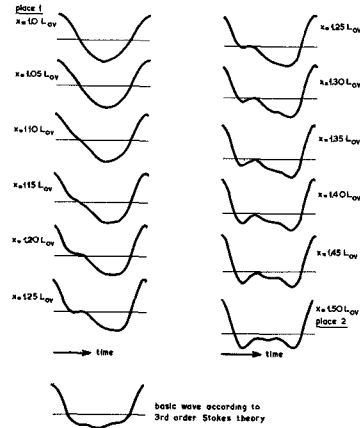


Figure 14: Theoretical wave forms for $h/L_1 = 0.10$ and $A_1/h = 0.18$

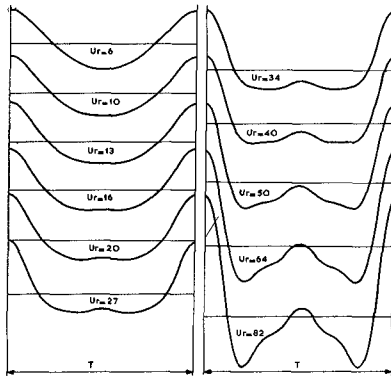


Figure 16: Wave forms at $x = (1/2 + k) L_{av}$ reconstructed from figure 15

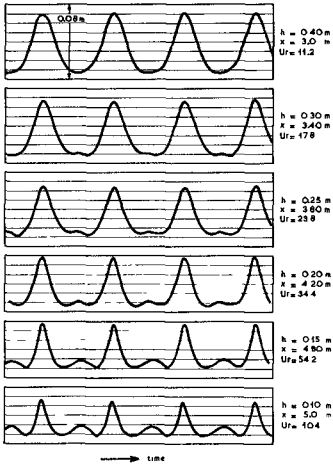


Figure 17: Experimental wave forms for $T = 1.92 \text{ s}$ at $x = 1/2 L_{OV}$

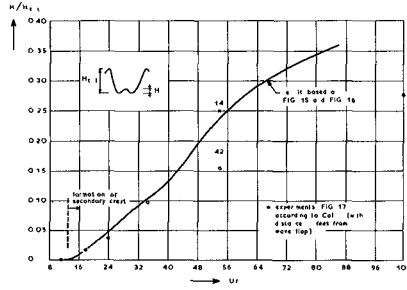


Figure 18: Relative height of secondary crest at $x = (1/2 + k)L_{OV}$

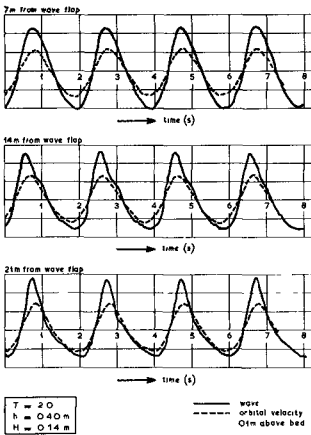


Figure 19: Simultaneous wave and orbital velocity

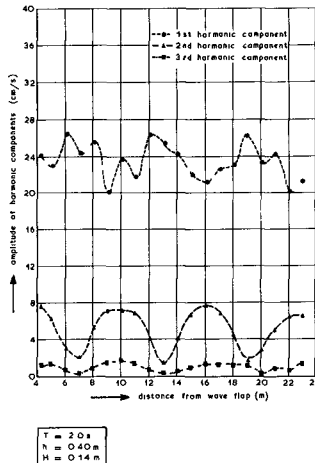
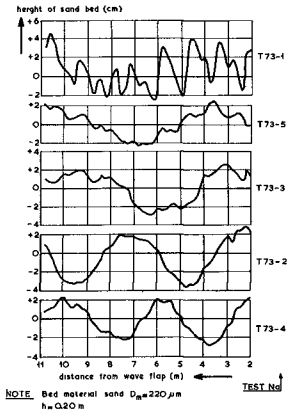


Figure 20: Spatial behaviour of harmonic amplitudes in orbital velocity



NOTE: Bed material sand $D_{50} = 220 \mu\text{m}$
 $h = 0.20 \text{ m}$

Test No.	T	H	Duration of test	L_w	L_{gr}
T73-1	198 s	5.4 cm	7 hrs	2.68 m	5.0 m
T73-2	180 s	8.0 cm	6 hrs 30 min	2.12 m	5.0 m
T73-3	178 s	7.6 cm	7 hrs	2.38 m	5.2 m
T73-4	185 s	8.6 cm	4 hrs	1.95 m	3.9 m
T73-5	188 s	7.0 cm	7 hrs	2.54 m	7.0 m

Figure 21: Influence of secondary waves on an initially flat horizontal bed

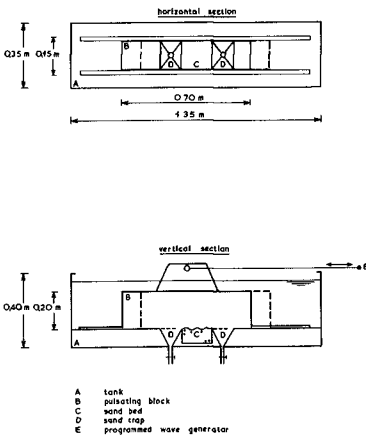


Figure 23: Pulsating water block

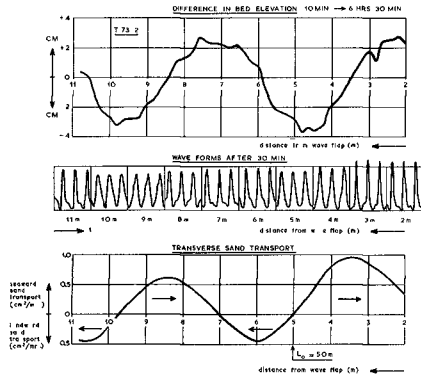


Figure 22: Typical wave forms and resulting sand transport

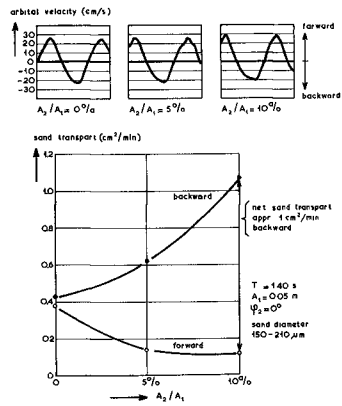


Figure 24: Influence of 2nd harmonic component on orbital velocity and sand transport

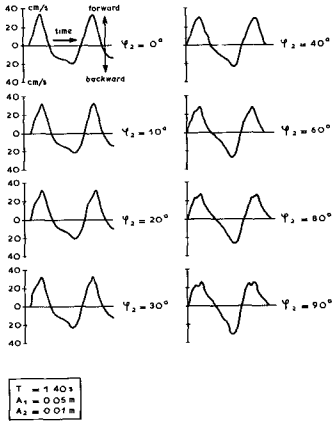


Figure 25. Velocity of pulsating block with variable ψ_2

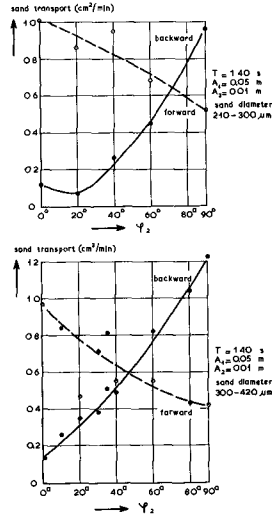


Figure 26. Influence of phase of 2nd harmonic component on sand transport

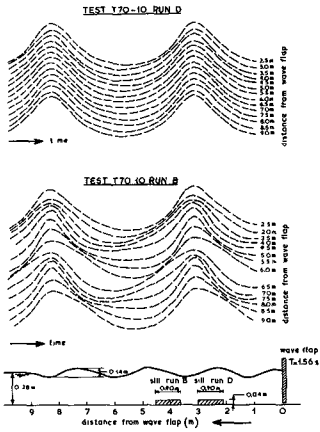


Figure 27: Typical wave form variation as influenced by location of low sill

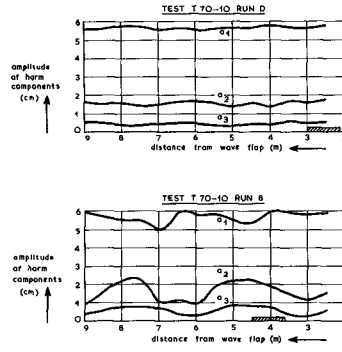


Figure 28: Harmonic amplitude variation as influenced by location of sill